Termination-dependent surface in-gap states in a potential mixed-valent topological insulator: SmB_6

Junwon Kim,[1] Kyoo Kim,[1] Chang-Jong Kang,[1] Sooran Kim,[1] Hong Chul Choi,[1] J.-S. Kang,[2] J. D. Denlinger,[3] and B. I. Min[1,*]

[1]*Department of Physics, PCTP, Pohang University of Science and Technology, Pohang 790-784, Korea*

[2]*Department of Physics, The Catholic University of Korea, Bucheon 420-743, Korea*

[3]*Advanced Light Source, Lawrence Berkeley Laboratory, Berkeley, California 94720, USA*

(Received 2 May 2014; revised manuscript received 5 August 2014; published 18 August 2014)

We have investigated the surface states of a potential mixed-valent topological insulator SmB_6 based on first-principles density functional theory slab band structure analysis. We have found that metallic surface states are formed in the bulk band gap region, providing evidence for the topological insulating nature of SmB_6. The obtained surface in-gap states are quite different from those in existing reports in that they are formed differently depending on the Sm or B_6 surface termination, and are composed of mainly the Sm $4f$ state indicating the essentiality of including f electrons in describing the surface states. We have obtained the spin chiral structures of the Fermi surfaces, which are also in accordance with the topological insulating nature of SmB_6.

DOI: 10.1103/PhysRevB.90.075131 PACS number(s): 71.20.Eh, 71.15.Nc, 71.18.+y

I. INTRODUCTION

The low-temperature residual conductivity in a typical Kondo insulator SmB_6 has been a long-standing unresolved problem. In this respect, recent reports on the topologically protected metallic surface states in SmB_6 have attracted much attention [1–11]. Angle-resolved photoemission spectroscopy (ARPES) can provide direct evidence for topological insulators via observation of the Fermi surfaces arising from the surface in-gap states. Indeed, Fermi surfaces were observed in several ARPES studies at $\bar{\Gamma}$ and $\bar{X}$ points of the surface Brillouin zone (BZ) [2,3,12,13], supporting the topological Kondo insulating nature of SmB_6. Unfortunately, however, no explicit Dirac cone feature has been observed. Hence, some groups interpreted the metallic states observed in ARPES not as topological surface states but as bulk-shifted or normal (trivial) surface states [13,14]. Especially, the origin of the metallic bands at $\bar{\Gamma}$ and $\bar{X}$ is controversial as to whether they come from bulk or surface states [2,3,5,12,13]. Above all, the spin polarizations of the metallic surface bands have not been unveiled yet [4,15].

Among many difficulties, the surface instability in SmB_6 prevents revealing the topological nature. Since the chemical bonding between Sm and B_6 ions is not weak, the natural cleavage plane in SmB_6 is not well defined. The pristine Sm- and B_6-terminated surfaces, which are electrically polar and highly reactive, are likely to undergo disordered reconstructions or contaminations [16–18]. Due to this reason, the topological nature arising from the intrinsic surface states is not easily confirmed experimentally. Another difficulty with SmB_6 is the strong correlation effect of f electrons. The highly renormalized f bands require extremely high resolution ARPES experiments. Nevertheless, the topological invariance of SmB_6, which has been confirmed by a couple of theoretical studies [9,11], arouses great curiosity about the characteristics of the metallic surface states in SmB_6 [19].

There have been a few surface band calculations which tried to identify the topological properties of SmB_6. Takimoto [9] and Lu *et al.* [11] performed the (001) surface model calculations based on the density functional theory (DFT) and the DFT+Gutzwiller bulk band structures, respectively. Both of them obtained the metallic surface states in the bulk gap region, which produce three Dirac cones and the corresponding Fermi surfaces at $\bar{\Gamma}$ and $\bar{X}$. This feature suggests the nontrivial topological nature of SmB_6. But they considered neither the surface termination dependence nor the surface relaxation effect. Zhu *et al.* [14] performed the DFT slab calculations, and also obtained the surface states in the vicinity of the Fermi level (E_F). But their surface states come from the polarity-driven boron dangling bond, and so they claimed that the metallic surface states in SmB_6 are not the topologically protected surface states but the normal surface states. In their surface slab calculations, however, they considered the Sm f electrons as core. Since the f-d hybridization is essential to develop the insulating state in bulk SmB_6, it is likely that their surface band structures are not relevant to the f-electron system of SmB_6.

In this article, we have investigated systematically the (001) surface states of a potential mixed-valent topological insulator SmB_6, using first-principles DFT calculations on the slabs with different surface terminations. We have first compared the bulk band structures obtained by the DFT with those obtained by the dynamical mean-field theory (DMFT), whereby we have shown that the DFT is useful to investigate the low-energy band structure of strongly correlated mixed-valent insulator SmB_6. Then, we have performed the DFT surface band structure calculations, and found that the surface bands and the corresponding Fermi surfaces are quite different from those in the literature [9,11,14]. The gapless surface states are formed differently for the Sm- and B_6-terminated surfaces. Moreover, additional surface states appear around $\bar{M}$ for the Sm-terminated case. We thus argue the importance of considering the Sm f electrons and the termination dependence in describing the surface states of SmB_6. Further, we have carefully examined the spin chiralities of the Fermi surfaces to corroborate the topological insulating nature of SmB_6.

II. COMPUTATIONAL DETAILS AND THE STRUCTURAL RELAXATION

SmB_6 crystallizes in a cubic structure of CaB_6 type with space group $Pm\bar{3}m$ (No. 221) and the lattice constant of

*bimin@postech.ac.kr

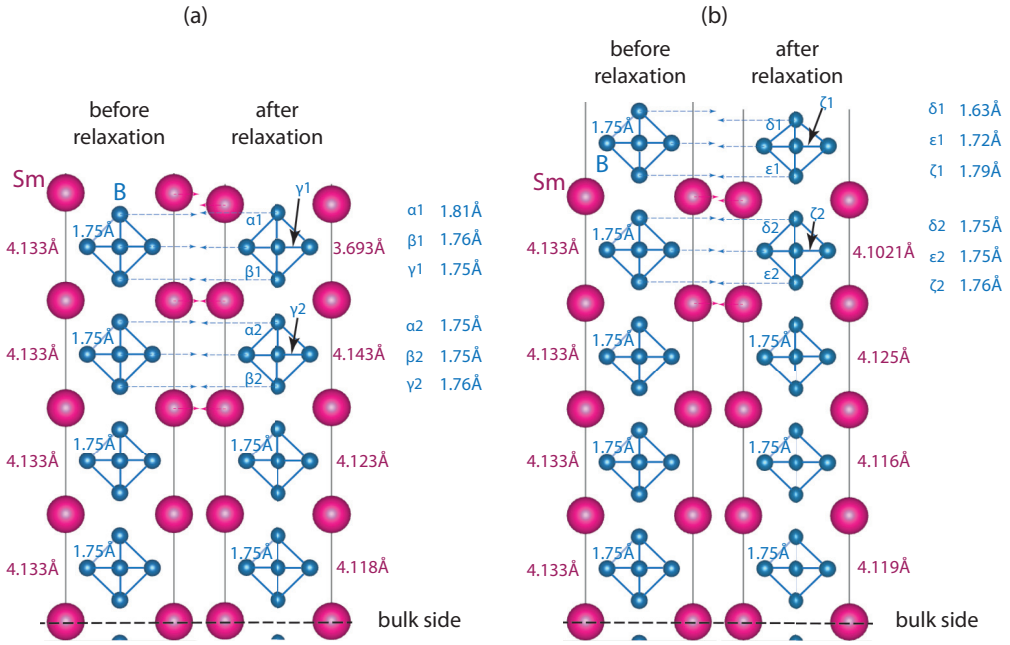

FIG. 1. (Color online) Relaxed structures of SmB_6 slabs having (a) Sm- and (b) B_6-terminated surfaces. After the structural relaxation, the thicknesses of both slabs are reduced. The structural relaxations were performed by using the VASP code.

4.133 Å. We have investigated the electronic structures of bulk SmB_6 using both the DFT and the DMFT incorporating the spin-orbit coupling (SOC). We used the DFT+DMFT scheme [22], implemented based on WIEN2K [20]. Coulomb and exchange interaction parameters were set by 7.00 eV and 0.83 eV, respectively, which were chosen to describe the known *f*-state multiplet structures from XPS data properly. For the impurity solver of the DMFT, we used both the noncrossing approximation (NCA) and the one-crossing approximation (OCA) [22]. It has been well tested for *f*-electron systems that the OCA captures well the correlated nature of *f* electrons [23]. For SmB_6, we checked that the band structure of the NCA is quite similar to that of the OCA.

Details of the electronic structure calculations for slab geometries of SmB_6 are as follows. For the DFT, we used both the full-potential linearized augmented-plane-wave (FLAPW) band method implemented in WIEN2K [20] and the projector-augmented wave (PAW) band method implemented in VASP [21]. In both cases, we have employed the generalized gradient approximation (GGA) for the exchange-correlation potential. Bond lengths and internal atomic positions were optimized using the conjugate-gradient algorithm implemented in the VASP code until the residual forces were less than 0.01 eV/Å. For the plane-wave bases, the energy cutoff of 320 eV was used. For the given relaxed structures obtained via VASP, we used both VASP and WIEN2K to cross-check the density of states (DOS) and band structures. In WIEN2K calculations, wave functions inside the muffin-tin (MT) spheres were expanded in the spherical harmonics up to $l_{\max} = 10$. The wave function in the interstitial region was expanded in the plane waves up to $K_{\max} \times R_{MT} = 7.0$ (R_{MT}: MT radius). R_{MT}'s of Sm and B are chosen as 2.5 a.u. and 1.5 a.u., respectively. $24\times24\times2$ **k**-point mesh was used in the Brillouin zone. To scrutinize the spin chirality of each Fermi surface originating from the surface states, the spin-noncollinear calculations were performed. To describe the surface states, two nonstoichiometric supercell geometries were employed, as shown in Figs. 1(a) and 1(b): (a) 9 Sm layers and 8 B_6 layers for the Sm-terminated slab, (b) 9 Sm layers and 10 B_6 layers for the B_6-terminated slab. In both cases, vacuum regions with 25 and 28 Å thickness, respectively, are considered in-between adjacent slabs. The resulting relaxed structures are shown in Figs. 1(a) and 1(b). In both cases, the slabs are seen to be shrunk mainly within two topmost layers.

III. RESULTS AND DISCUSSION

DMFT band structures in Fig. 2 demonstrate the temperature (T) dependent f-d hybridization behavior. At high $T = 150$ K in Fig. 2(b), Sm f electrons do not form coherent bands, and so the metallic Sm d band crossing E_F is clearly visible around X, reflecting little hybridization with incoherent f bands. Upon cooling, the f electrons form the coherent bands that become strongly hybridized with the d band so as to display a gap feature, even though the gap size is almost zero in the DMFT result of Fig. 2(a) ($T = 5$ K).

In Fig. 2(a), the DMFT bands are overlaid with DFT bands that are rescaled down in energy by 1/10 (thin dotted blue). It is seen that the DMFT and DFT band structures near E_F are essentially the same as each other. This feature suggests that the strong correlation effect of f electrons can be captured to some extent just by renormalizing DFT bands. The gap feature persists in the renormalized DFT band structure with a reduced size of ~2 meV with respect to the original gap size of ~20 meV. Of course, the renormalized DFT cannot simulate the Sm $j = 7/2$ bands that are to be shifted up by the strong correlation of Sm $4f$ electrons. So the position of Sm $j = 7/2$ bands in the DFT is located much closer to E_F than in the DMFT. In fact, the present authors have previously analyzed the influence of the low-lying Sm $j = 7/2$ bands on the states

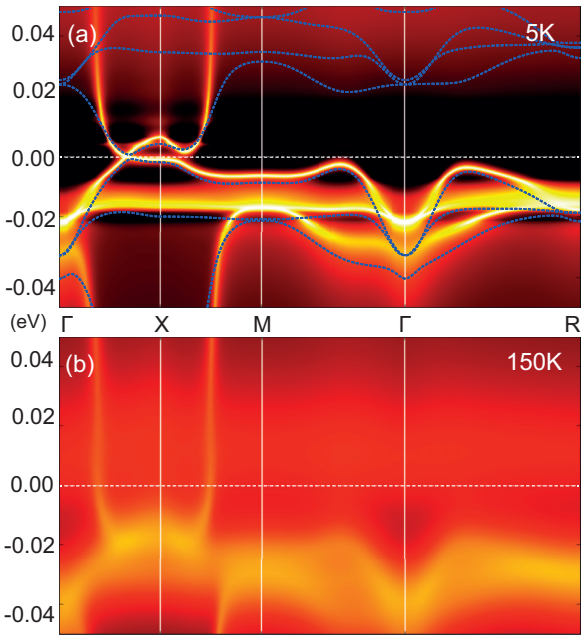

FIG. 2. (Color online) Momentum-resolved spectral function of SmB_6 obtained by the DFT+DMFT method at (a) $T = 5$ K and (b) $T = 150$ K. Transition to the metallic state is clearly visible at higher temperature 150 K [5]. The GGA band structure (blue solid lines), which is rescaled by 1/10, is overlaid on the DMFT band structure.

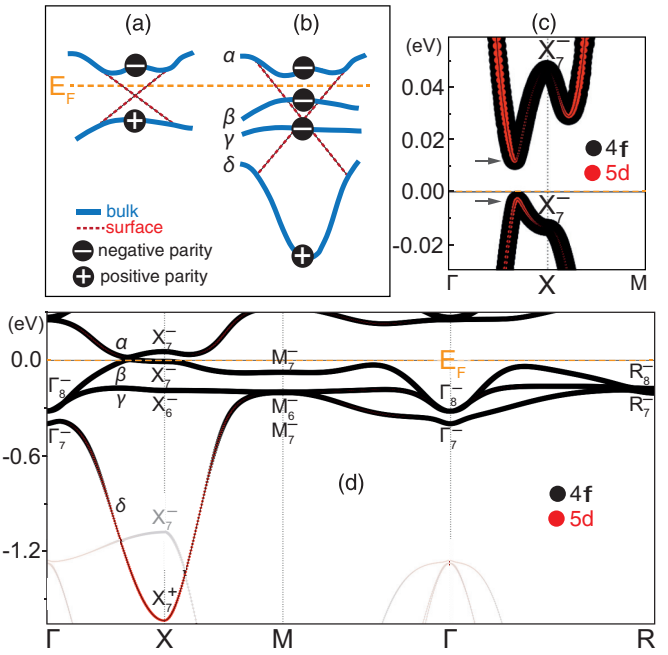

FIG. 3. (Color online) Schematic pictures showing (a) usual and (b) unusual band inversions. In SmB_6, parity-inverted bands are α and δ, but two more bands β and γ are located between them. (c) In SmB_6, the DFT bands just below and above E_F do not show band inversion at X, because both of them have the f-orbital character having the negative parity. Black and red dots represent the weights of Sm $4f$ and $5d$ components, respectively. (d) DFT bulk band structure of bulk SmB_6. As shown in (b), two more bands with negative parity are located below E_F.

near E_F for bulk SmB_6 [24]. This effect will be discussed more at the end of the section.

In typical topological insulators such as Bi_2Se_3 or Bi_2Te_3, the parity inversion occurs at a high symmetry point between two bulk bands having different parities, and the topologically protected surface states emerge in the gap region, as shown in Fig. 3(a). SmB_6, however, shows a peculiar parity inversion feature. As discussed in Fig. 2, the occurrence of the gap in SmB_6 is initiated by the f-d hybridization near X, but the band gap is seen to be realized between two f bands, as shown Figs. 3(b)–3(d). Namely, there are two more f bands, β and γ, having the same negative parity (X_7^-) in-between parity-inverted bands of α (X_7^-) and δ (X_7^+). Therefore, some part of the surface in-gap states including the Dirac point would be buried in the bulk β and γ bands, as in Fig. 3(b). This feature in SmB_6 is different from the usual topological insulators, in which the Dirac cone features are clearly observed in the gap region. This is an important difference, making SmB_6 more complicated than other conventional topological insulators.

In order to probe into the surface states of SmB_6, we have performed the DFT slab calculations for both Sm- and B_6-terminated (001) surfaces, including Sm f electrons as valence electrons. Figures 4(a) and 4(b) show the surface states of Sm- and B_6-terminated SmB_6 slabs, respectively. In both cases, there appear metallic surface states in the bulk gap region, which are seen to merge into bulk bands projected to the surface BZ. The surface in-gap states here are composed of mainly the Sm f state (the weight of the f component is more than 90%). This result is quite contrary to the previous DFT surface band calculation [14], in which the surface states near E_F came mostly from the B $2p$ dangling bond state. This discrepancy arises from that Sm f electrons were not taken into account as valence electrons in Ref. [14]. Without Sm f electrons, we also obtained the B $2p$ surface states that cross E_F [26]. However, in this case, there are many other metallic bands near E_F besides the B $2p$ surface bands due to the lack of hybridization with f electrons, which is certainly in disagreement with ARPES data. Note that the B $2p$ surface states do not satisfy the criterion of the topological insulator, whereas the present surface states including Sm f electrons do on both terminations. Thus the inclusion of f electrons as valence state changes the situation near E_F dramatically.

At a glance, the surface states in Fig. 4(b) for the B_6-terminated case look analogous to those obtained by the tight-binding (TB) surface model calculation based on the LDA+Gutzwiller bulk band result [11]. However, there are interesting differences. First, in the TB result, the gapless surface states, especially at $\bar{X}$, seem to be generated from the band β manifesting the Dirac points in the gap region, while, in the present rescaled DFT, the Dirac point is seen to be just buried in the band β. This is not a minor distinction. Since the parities of bulk band β and γ are negative, the absence of both bands does not change the topological order. So the gapless surface states are not formed via the bulk band β and γ, but formed just passing through both bands [27]. Interestingly, a similar feature of a buried Dirac point in the bulk bands is also seen in PuB_6, which was reported to be a correlated topological insulator [28].

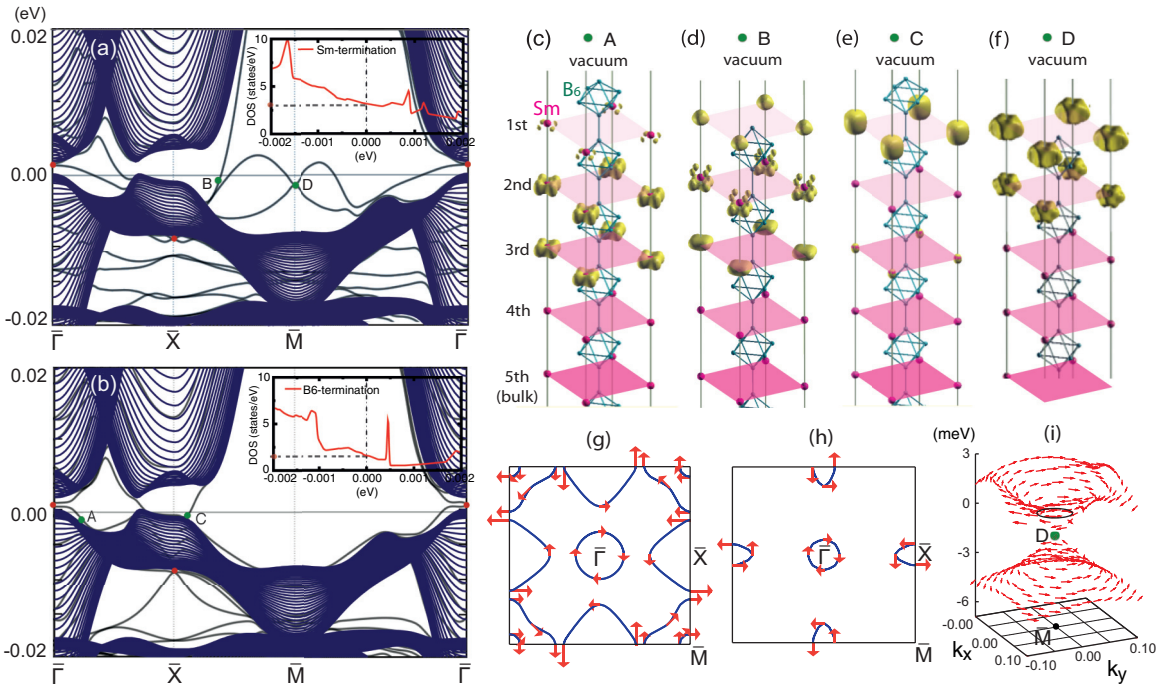

FIG. 4. (Color online) DFT band structures of SmB_6 slabs with (a) the Sm-terminated surface and (b) the B_6-terminated surface. Note that the energy scales in (a) and (b) are reduced by 1/10. Blue shaded region represents the projection of SmB_6 bulk bands to the (001) surface BZ. Red dots represent the crossing (Dirac) points of metallic surface bands. Insets show the total DOS divided by the number of Sm layers of each surface termination [25]. (c)–(f) Charge densities of wave functions at given points A, B, C, and D (green dots) of the metallic surface bands. (g), (h) Fermi surfaces of the Sm and the B terminations, respectively. Spin helicity in each Fermi surface is plotted with red arrow. (i) Dirac-cone-like shape of the spin chiral texture of the surface state at $\bar{M}$. Charge densities in (c)–(f) are drawn based on the WIEN2K data, while all the others are drawn based on the VASP data.

Second, Sm-termination in Fig. 4(a) shows additional surface in-gap states centered at $\bar{M}$, which have never been recognized theoretically. The existence of these metallic surface states does not violate the E_F crossing criterion of Z_2 topological characterization. The different surface states depending on the terminations are quite natural even in conventional topological insulators [29]. It is, however, rarely reported in real materials that additional metallic surface states emerge with different dispersions at another high symmetry point. Metallic surface states centered at $\bar{M}$ have not been reported experimentally either. One reason why $\bar{M}$-centered surface states have not been detected might be due to the fact that the size of a well-ordered 1×1 Sm-terminated surface known until now is not over a few nanometers [17,18]. The beam spot size of state-of-the-art ARPES may not be enough to capture the physics of such a small 1×1 ordered Sm-terminated surface.

Figures 4(c)–4(f) show the charge densities of surface wave functions at specific **k** points. It is shown that the charge densities of the surface states originate indeed from the surface atoms, mainly from Sm atoms, of both terminated slabs. It is worthwhile to note in Fig. 4(c) that the surface state near $\bar{\Gamma}$ (A) is quite discernible from other surface states near $\bar{X}$ and $\bar{M}$ (B, C, D), in that the dominant charge density at A is slightly away from the topmost layer and locates rather close to the bulk side. This is also the case for the surface state at $\bar{\Gamma}$ for the Sm termination. This feature suggests that the surface state at $\bar{\Gamma}$ could be more robust than other surface states against any changes at the surface.

Figures 4(g) and 4(h) present the Fermi surfaces (FSs) of surface states together with spin chiral structures. It is seen that both terminations have FSs at $\bar{\Gamma}$ and $\bar{X}$ with the same helical spin polarization, even though the FSs of the B_6-termination are smaller than those of the Sm-termination. In both cases, FSs at $\bar{\Gamma}$ and $\bar{X}$ are hole and electron FSs, respectively. Also, due to the surface states of the Sm-termination around $\bar{M}$, there appear additional FSs of flower shape centered at $\bar{M}$ for the Sm-termination case in Fig. 4(g). These FSs also have helical spin polarizations. The spin texture of the surface state at $\bar{M}$ is more specifically shown in Fig. 4(i), which reveals the opposite helicities above and below the Dirac point D. Therefore, not only previously reported surface states at $\bar{\Gamma}$ and $\bar{X}$ but also that at $\bar{M}$ has a Dirac-cone-like spin texture. This feature corroborates the topological nature of the surface states in SmB_6. One thing to be pointed out is that the $\bar{M}$-centered FSs could be fragile with respect to any environmental perturbations on the surface. It is because, even without the $\bar{M}$-centered FSs, the criterion for nontrivial topology, i.e., an odd number of E_F crossings, is still valid.

According to recent STM/STS [18] data on the nonreconstructed ordered Sm- and B_6-surface terminated SmB_6, the differential conductance of the former is about 30% larger than that of the latter at $T = 4.6$ K. This implies that there are additional conducting channels at the Sm-terminated surface, suggesting the higher DOS near E_F. Indeed, the insets of Figs. 4(a) and 4(b) show the surface DOSs, which are about 50% larger at E_F in the case of the Sm-terminated surface, which matches well with the

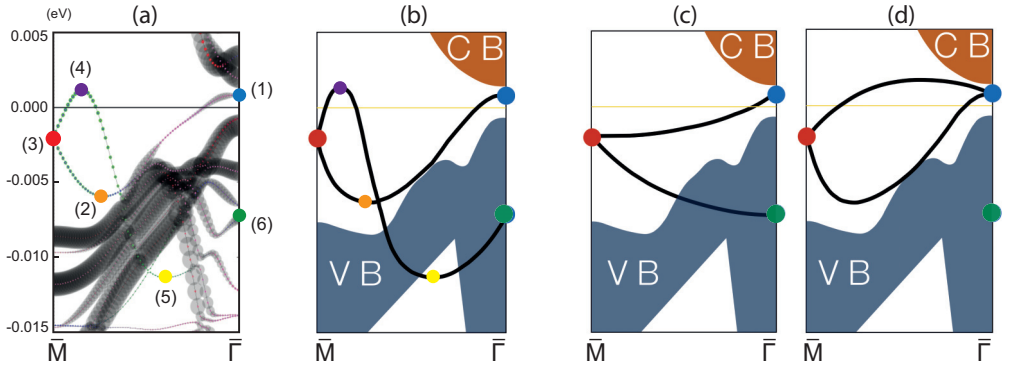

FIG. 5. (Color online) (a) The surface band structure along $\bar{M}$-$\bar{\Gamma}$ for the Sm-terminated SmB_6 slab. Thick black circles represent the weight contributions from bulk bands. To show the surface states distinctly, they are plotted with small colored circles that represent the weight contributions from surface B $2p$ states. (b) Schematic band structure of (a), which shows the switching of two surface bands. (c) Topologically nontrivial surface states in conventional topological insulators. (d) Topologically trivial surface states in conventional band insulators. CB and VB represent the projected bulk conduction and valence bands, respectively.

STS/STM result. So the metallic surface states at $\bar{M}$ can explain the larger differential conductance on the Sm-terminated surface.

Differently from $\bar{\Gamma}$- and $\bar{X}$-centered surface states in SmB_6, $\bar{M}$-centered surface states, which emerge only in the Sm-terminated SmB_6 for both VASP and WIEN2K band results, have not been explored in the context of topological insulators. In the topological insulators, Kramers degenerate pairs switch partners, reflecting the change in the time reversal polarization [30]. Also, the corresponding surface states cross the Fermi level (E_F) an odd number of times between TRIM (time reversal invariant momentum) points having different time reversal polarizations, -1 or 1. We checked the topological nature of the surface states at $\bar{M}$. It is seen that the upper band at $\bar{M}$ first increases in energy above E_F and then decreases down so as to be connected to the band (6) at $\bar{\Gamma}$ below E_F, while the lower band at $\bar{M}$ is connected to the band (1) at $\bar{\Gamma}$ above E_F, as is schematically drawn in Fig. 5(b). It shows typical features of topological insulators such as "switching partners" and "an odd number of E_F crossing" [Fig. 5(c)], which is clearly different from that of normal band insulators [Fig. 5(d)]. But the Dirac cone at $\bar{M}$ is seen to be reversed with respect to a normal Dirac cone in Fig. 5(c) that has monotonically decreasing or increasing dispersions.

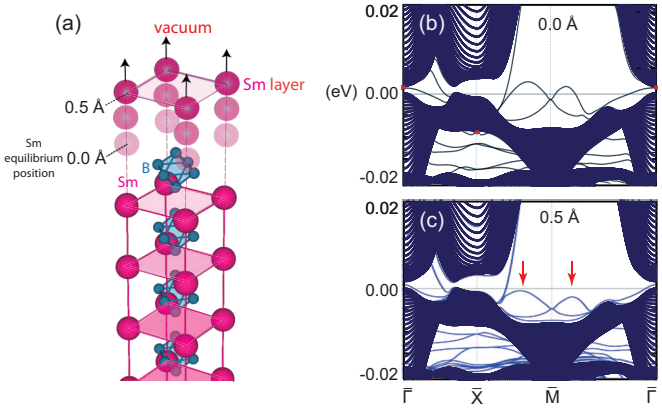

FIG. 6. (Color online) Variations of the topological surface states in the Sm-terminated SmB_6 with respect to a perturbation of lifting up the top Sm layer to vacuum side from its equilibrium position by 0.5 Å. A slab geometry of 11 Sm layers and 10 B_6 layers is used with 88 Å vacuum region in-between adjacent slabs. (b), (c) Surface states before and after the perturbation. Fermi surfaces centered at $\bar{M}$ disappear due to the perturbation, while those centered at $\bar{\Gamma}$ and $\bar{X}$ are intact.

To investigate the robustness of the Fermi surfaces, we examined the variation of the surface states with respect to a perturbation. For that purpose, we considered the situation that the top Sm layer of the Sm-terminated slab was shifted up from its equilibrium position by 0.5 Å [see Fig. 6(a)]. As shown in Figs. 6(b) and 6(c), due to this perturbation, two $\bar{M}$-centered Fermi surfaces disappear, while $\bar{\Gamma}$- and $\bar{X}$-centered Fermi surfaces are intact. The relevant surface states at $\bar{M}$ become less dispersive and the Dirac point becomes lower than before. This feature suggests that $\bar{M}$-centered Fermi surfaces are likely to be more fragile than $\bar{\Gamma}$- and $\bar{X}$-centered Fermi surfaces. Note that these two $\bar{M}$-centered Fermi surfaces are not compulsory for the topological insulating nature of SmB_6.

In our early investigation of bulk bands of SmB_6 using the DFT [24], we found that Sm $j = 7/2$ bands above E_F are mixed somehow with the low-lying f bands near E_F, so as to produce the spurious charge densities. Hence, to remove the influences of $j = 7/2$ bands around E_F, we performed the slab calculations with the 10 times stronger SOC, as we did in the bulk case. We have ascertained that the overall features of metallic surface states, such as number of FSs, relative FS sizes, and the hole or electron nature of each FS, are almost unchanged even with the stronger SOC for both terminations. This result indicates that the effects of Sm $j = 7/2$ bands on the metallic surface states of SmB_6 near E_F would be minor.

IV. CONCLUSION

We have investigated the surface in-gap states of SmB_6 based on first-principles DFT slab band structure analysis. We have found that (i) the surface states and corresponding FSs emerge at around $\bar{\Gamma}$ and $\bar{X}$, (ii) there appear additional

surface states centered at $\bar{M}$ for the Sm-termination case, and (iii) more importantly, the present surface states are quite different from those of existing surface band calculations, such as the TB slab calculation and the DFT calculation without considering Sm $4f$ electrons. We have also determined the spin helicities of Fermi surfaces, which are consistent with the topological Kondo insulating nature of SmB_6. For clear confirmation, spin-resolved ARPES on the ordered surface is strongly recommended.

ACKNOWLEDGMENTS

We would like to thank Jinwoong Kim and J. H. Shim for helpful discussions. This work was supported by the NRF (Grants No. 2009-0079947 and No. 2011-0025237), a POSTECH BSRI grant, and the KISTI supercomputing center (Grant No. KSC-2012-C3-055). J.S.K. acknowledges support by the NRF (Grant No. 2011-0022444). J.D.D. is supported by the U.S. DOE (Grant No. DE-AC02-05CH11231).

[1] S. Wolgast, Ç. Kurdak, K. Sun, J. W. Allen, D.-J. Kim, and Z. Fisk, Phys. Rev. B **88**, 180405(R) (2013).

[2] N. Xu, X. Shi, P. K. Biswas, C. E. Matt, R. S. Dhaka, Y. Huang, N. C. Plumb, M. Radovíc, J. H. Dil, E. Pomjakushina, K. Conder, A. Amato, Z. Salman, D. McK. Paul, J. Mesot, H. Ding, and M. Shi, Phys. Rev. B **88**, 121102(R) (2013).

[3] M. Neupane, N. Alidoust, S.-Y. Xu, T. Kondo, Y. Ishida, D.-J. Kim, C. Liu, I. Belopolski, Y. J. Jo, T.-R. Chang, H.-T. Jeng, T. Durakiewicz, L. Balicas, H. Lin, A. Bansil, S. Shin, Z. Fisk, and M. Z. Hasan, Nat. Commun. **4**, 2991 (2013).

[4] C.-H. Min, P. Lutz, S. Fiedler, B. Y. Kang, B. K. Cho, H.-D. Kim, H. Bentmann, and F. Reinert, Phys. Rev. Lett. **112**, 226402 (2014).

[5] J. D. Denlinger, J. W. Allen, J.-S. Kang, K. Sun, J.-W. Kim, J. H. Shim, B. I. Min, D.-J. Kim, and Z. Fisk, arXiv:1312.6637.

[6] Wei Ruan, Cun Ye, Minghua Guo, Fei Chen, Xianhui Chen, Guang-Ming Zhang, and Yayu Wang, Phys. Rev. Lett. **112**, 136401 (2014).

[7] F. Chen, C. Shang, A. F. Wang, X. G. Luo, T. Wu, and X. H. Chen, arXiv:1309.2378.

[8] M. Dzero, K. Sun, V. Galitski, and P. Coleman, Phys. Rev. Lett. **104**, 106408 (2010).

[9] T. Takimoto, J. Phys. Soc. Jpn. **80**, 123710 (2011).

[10] M. Dzero, K. Sun, P. Coleman, and V. Galitski, Phys. Rev. B **85**, 045130 (2012).

[11] F. Lu, J. Z. Zhao, H. Weng, Z. Fang, and X. Dai, Phys. Rev. Lett. **110**, 096401 (2013).

[12] H. Miyazaki, T. Hajiri, T. Ito, S. Kunii, and S.-I. Kimura, Phys. Rev. B **86**, 075105 (2012).

[13] E. Frantzeskakis, N. de Jong, B. Zwartsenberg, Y. K. Huang, Y. Pan, X. Zhang, J. X. Zhang, F. X. Zhang, L. H. Bao, O. Tegus, A. Varykhalov, A. de Visser, and M. S. Golden, Phys. Rev. X **3**, 041024 (2013).

[14] Z.-H. Zhu, A. Nicolaou, G. Levy, N. P. Butch, P. Syers, X. F. Wang, J. Paglione, G. A. Sawatzky, I. S. Elfimov, and A. Damascelli, Phys. Rev. Lett. **111**, 216402 (2013).

[15] S. Suga, K. Sakamoto, T. Okuda, K. Miyamoto, K. Kuroda, A. Sekiyama, J. Yamaguchi, H. Fujiwara, A. Irizawa, T. Ito, S. Kimura, T. Balashov, W. Wulfhekel, S. Yeo, F. Iga, and S. Imada, J. Phys. Soc. Jpn. **83**, 014705 (2014).

[16] M. Trenary, Sci. Technol. Adv. Mater. **13**, 023002 (2012).

[17] M. M. Yee, Y. He, A. Soumyanarayanan, D.-J. Kim, Z. Fisk, and J. E. Hoffman, arXiv:1308.1085.

[18] S. Rößler, T.-H. Jang, D. J. Kim, K. H. Tjeng, Z. Fisk, F. Steglich, and S. Wirth, Proc. Natl. Acad. Sci. USA **111**, 4798 (2014); J. Phys. Soc. Jpn. **83**, 014705 (2014).

[19] Z. K. Liu, Y. L. Chen, J. G. Analytis, S. K. Mo, D. H. Lu, R. G. Moore, I. R. Fisher, Z. Hussain, and Z. X. Shen, Physica E **44**, 891 (2012).

[20] B. Blaha, K. Schwarz, G. K. H. Madsen, D. Kvasnicka, and J. Luitz, WIEN2K, *An Augmented Plane Wave Plus Local Orbitals Program for Calculating Crystal Properties* (Vienna University of Technology, Austria, 2001).

[21] VASP code, http://www.vasp.at.

[22] K. Haule, C.-H. Yee, and K. Kim, Phys. Rev. B **81**, 195107 (2010).

[23] Hong Chul Choi, B. I. Min, J. H. Shim, K. Haule, and G. Kotliar, Phys. Rev. Lett. **108**, 016402 (2012).

[24] C.-J. Kang, J. Kim, K. Kim, J.-S. Kang, J. D. Denlinger, and B. I. Min, arXiv:1312.5898.

[25] We can ignore the difference of the number of boron layers because more than 90% of the total DOS comes from the Sm layers in this energy window.

[26] Other B $2p$ surface states at about -2.0 eV for the Sm-terminated case remain almost unchanged even after the inclusion of the f electrons.

[27] S.-Y. Lee, J.-H. Park, G. Go, and J. H. Han, arXiv:1312.6469.

[28] X. Deng, K. Haule, and G. Kotliar, Phys. Rev. Lett. **111**, 176404 (2013).

[29] Q. D. Gibson, L. M. Schoop, A. P. Weber, Huiwen Ji, S. Nadj-Perge, I. K. Drozdov, H. Beidenkopf, J. T. Sadowski, A. Fedorov, A. Yazdani, T. Valla, and R. J. Cava, Phys. Rev. B **88**, 081108(R) (2013).

[30] Liang Fu, C. L. Kane, and E. J. Mele, Phys. Rev. Lett. **98**, 106803 (2007).